RSC Advances

PAPER

View Article Online
View Journal | View Issue

Cite this: *RSC Adv.*, 2024, **14**, 26354

Efficient antimicrobial applications of two novel supramolecular metallogels derived from a L(+)-tartaric acid low molecular weight gelator†

Subhendu Dhibar, ‡*[a] Suchetana Pal,‡[b] Sangita Some,[a] Kripasindhu Karmakar,[a] Ratnakar Saha,[c] Subham Bhattacharjee,[d] Arpita Roy,[e] Soumya Jyoti Ray,[e] Timothy O. Ajiboye,[f] Somasri Dam*[b] and Bidyut Saha*[a]

Received 10th May 2024
Accepted 9th August 2024

DOI: 10.1039/d4ra03451a

rsc.li/rsc-advances

Novel metallogels were synthesized using L(+)-tartaric acid as a gelator, along with cadmium(II)-acetate and mercury(II)-acetate in *N*,*N*-dimethyl formamide at room temperature. Rheological analyses confirmed the mechanical stability of Cd(II)- and Hg(II)-metallogels under varying conditions. Characterization through EDX mapping and FESEM imaging provided insights into their chemical constituents and microstructural features. FT-IR spectroscopy elucidated the metallogel formation mechanism. Antimicrobial assays revealed significant activity against various bacteria, including Gram-positive and Gram-negative strains. This study presents a comprehensive exploration of Cd(II) and Hg(II)-based L(+)-tartaric acid-mediated metallogels, highlighting their potential in combating bacterial infections. These findings suggest promising applications in both industrial and biomedical fields, offering avenues for the development of advanced materials.

1. Introduction

Gel constitutes a three-dimensional lattice of polymers interconnected through cross-links, effectively trapping solvent molecules with the aid of gelator molecules.[1] The synthesis and design of gels are characterized by their unpredictability and intrigue, often stemming from serendipitous formation processes.[2] For instance, the identification of a gel can be achieved through a simple inversion vial test, where its ability to maintain its structure against gravity is observed.[3] Various forms of gel are ubiquitous in our daily lives, integrated into a myriad of products such as shampoo, soap, contact lenses, ointments, cosmetics, and countless others, underscoring their diverse applications and indispensable role in everyday use.[4] Gels can be divided into two categories based on their interactions: chemical gels,[5] which form through robust covalent bonding, and supramolecular gels,[5] which arise from the self-assembly[6] of low molecular weight gelators (LMWGs).[7] These LMWGs, with a molecular weight typically less than 3000, utilize various non-covalent interactions such as π–π stacking,[8] hydrogen bonding,[9] van der Waals forces,[10] hydrophilic and hydrophobic interactions,[9,11] dipole–dipole interactions,[12] ion–dipole interactions,[12] π-ring mediated interactions,[13] and π-system based stacking.[13] Effective gelators for supramolecular gels include dibasic acids,[14] urea,[15] modified amino acids,[16] carbohydrates,[17] amides,[18] alkenes,[19] stearic acid,[14] sorbitol,[17] fatty acids,[5] dendrimers,[17] and more. The choice of solvent plays a crucial role in triggering gel formation, influencing gel morphology through factors like polarity, viscosity, and interactions with ligands and metal ions. Both organic and inorganic solvents can efficiently induce gel formation, depending on the nature of the gelators.[20] Water,[21] alcohols,[21] dimethylformamide,[22] dimethyl sulfoxide,[23] 1,2-dichlorobenzene,[24] acetonitrile,[25] acetone,[26] toluene,[27] dichloromethane,[28] and deuterated dichloromethane[29] are among the most effective solvents for initiating supramolecular gel formation. Interestingly, solvents themselves can sometimes act as gelator molecules.[30,31] Through their weak non-covalent interactions, they can facilitate a reversible transition between the gel and sol phases, influenced by external factors such as mechanical forces, pH, temperature, and electrolytes.[32] Supramolecular gels offer intriguing potential across diverse fields such as drug delivery,[33] tissue regeneration scaffolds,[34] catalysis,[35] soft robotics,[36] and environmental applications like pollutant absorption and

[a]*Colloid Chemistry Laboratory, Department of Chemistry, The University of Burdwan, Golapbag, Burdwan 713104, West Bengal, India. E-mail: sdhibar@scholar.buruniv.ac.in; bsaha@chem.buruniv.ac.in; Tel: +91 7001575909; +91 9476341691*

[b]*Department of Microbiology, The University of Burdwan, Burdwan 713104, West Bengal, India. E-mail: sdam@microbio.buruniv.ac.in*

[c]*National Institute of Science Education and Research (NISER), Bhubaneswar, Odisha 752050, India*

[d]*Department of Chemistry, Kazi Nazrul University, Asansol 713303, West Bengal, India*

[e]*Department of Physics, Indian Institute of Technology Patna, Bihar 801106, India*

[f]*Department of Chemistry, University of the Free State, Bloemfontein, 9301, South Africa*

† Electronic supplementary information (ESI) available. See DOI: https://doi.org/10.1039/d4ra03451a

‡ SD and SP should be treated as joint first authors.

controlled chemical release.[37] These gels are particularly attractive due to their characteristic properties such as self-healing,[38] responsiveness to stimuli,[6] and shear-thinning behavior.[39]

Supramolecular metallogels represent a specialized category within the broader class of supramolecular gels, arising from the self-assembly of metal ions or metal complexes with organic ligands (LMWGs) to form intricate three-dimensional networks.[40] These networks are stabilized not only by typical non-covalent interactions like hydrogen bonding,[9] π–π stacking,[41] and van der Waals forces[10] but also by coordination bonding interactions[4] between the metal centers and the ligands.[42] The unique characteristics of supramolecular metallogels can be finely tuned by selecting specific metal ions and ligands and by manipulating the surrounding environment. Transition metal-based metallogels have garnered considerable attention from researchers due to their cost-effectiveness, accessibility, and enhanced ability to coordinate with organic ligands. Numerous metallogels employing a variety of metal ions such as Cu(II),[43] Ni(II),[44] Co(II),[45] Zn(II),[46] Fe(II/III),[47] Cd(II),[48] Hg(II),[48] and Mn(II)[21] have been synthesized, showcasing their versatility and potential applications. These metallogels find wide-ranging utility in catalysis,[35] conduction,[49] magnetism,[50] redox reactions,[51] and nanoparticle templating,[52] owing to the pivotal role of metals within the network structure. Ligands, particularly dicarboxylic acids, play a crucial role in these systems due to their strong interactions with transition metals. The carboxylate groups in dicarboxylic acids coordinate with metal ions, forming complexes that are essential for promoting gelation. This makes dicarboxylic acids important in metallogel research, as they are key drivers in the formation of metal–ligand networks. Tartaric acid, an organic compound with two carboxylic acid groups and two hydroxyl groups, is a particularly effective low molecular weight gelator (LMWG). Its molecular structure enables extensive hydrogen bonding, both intra- and intermolecular, which facilitates the formation of stable networks crucial for the gelation of solvents or co-solvents.[43] Researchers have explored diverse applications of metallogels, including chemotherapy,[53] photodynamic therapy,[54] cell imaging,[34] and antibacterial activity,[49] leveraging the distinctive properties conferred by different metal ions. A nanohybrid metallogel comprising of peptide gel-based nanofibers and silver NC/NPs have been reported to have potential antimicrobial activity.[55] Supramolecular metallogel from suberic acid and the metals nickel, zinc and cadmium are known to have potential antibacterial efficiency.[56] Ni(II) and Zn(II)-metallogels have antibacterial property against various human pathogens.[57] Metallogel based on metal–phenolic coordination of natural low-cost polyphenolic molecule and metal ions was found to be effective as dressings for infected wounds.[58] Previous studies have reported the use of succinic acids,[59] oxalic acids,[40] and adipic acids[4] in mediating gels with specific applications and low toxicity. L(+)-Tartaric acid, known for its widespread use as a flavoring and preservative in food and beverages, also serves as an antibacterial agent and antioxidant.[60,61] Its unique properties enable the formation of high aspect ratio functional supramolecular metallogels, further expanding the scope of potential applications. Recent research efforts have also highlighted the antibacterial activity of Cd(II)-based systems and the significance of Hg(II)-directed materials in biological systems, underscoring the diverse and promising avenues of exploration in metallogel research.[49,62] Conversely, there are documented instances of Cd and Hg inducing cellular toxicity. Cd can disrupt the cellular energy processes in human bone cells, triggering oxidative stress through the generation of free radicals and hindering the natural antioxidant defenses of the cell.[63] The cytotoxic effects of Hg and Cd on human peripheral immune cells became permanent after a significant amount of time. The exposure of Hg and Cd causes serious destruction of the cell membrane.[64]

Drawing inspiration from emerging trends, our research delves into the impact of metallogel scaffolds on combating pathogens. Specifically, we focus on the metallo-gelation potential of L(+)-tartaric acid with Cd(II) and Hg(II) sources in *N*,*N*-dimethylformamide solvent under ambient conditions. L(+)-Tartaric acid, a low molecular weight gelator (LMWG), serves as the driving force behind the formation of two novel supramolecular metallogels: Cd(II)–L-(+) tartaric acid metallogel (Cd–TA) and Hg(II)–L-(+) tartaric acid metallogel (Hg–TA). To assess the mechanical properties of the synthesized metallogels, we conducted rheological analyses. Additionally, we utilized field emission scanning electron microscopy (FESEM) to reveal the morphological patterns of the metallogels and employed energy-dispersive X-ray (EDX) mapping investigations to characterize the chemical constituents. The rampant use of conventional antibiotics has led to the emergence of drug-resistant organisms, necessitating the urgent development of novel antimicrobial agents. Metallogel moieties present promising candidates for inhibiting bacterial growth, making them particularly appealing in biomedical applications. The biological applications of L(+)-tartaric acid further drive our investigation into the anticipated bio-functionality of L(+)-tartaric acid and various metal ion-based metallogel systems. Our current efforts have demonstrated the anti-bacterial efficacy of L(+)-tartaric acid-based metallogels of Cd(II) and Hg(II), showcasing their potential as innovative solutions in the fight against microbial infections.

2. Experimental

2.1. Materials

Cadmium(II) acetate dihydrate (99.995%), mercury(II) acetate (≥98.0%), L-(+) tartaric acid and DMF were obtained from Merck Chemical Company and utilized without additional purification. Dry DMF solvent was employed consistently throughout the experimentation. Tryptone, D-(+)-glucose anhydrous, and Yeast Extract Powder were procured from Himedia.

2.2. Apparatus and measurements

The metallogel synthesis utilized the Phoenix Digital Ultrasonic Cleaner PHUC-150. Rheological analysis was conducted using a cone-plate rheometer from TA Instruments. Field emission scanning electron microscope (FESEM) investigations were

performed with a Carl Zeiss SUPRA 55VP FESEM instrument. Scanning mode energy-dispersive X-ray spectroscopy (EDX) studies were carried out using the ZEISS EVO 18 apparatus. Topography analysis was conducted using an atomic force microscope (Agilent Technology 5500) in noncontact mode with a silicon tip. The FTIR spectrum of the metallogel was analyzed using a JASCO FTIR 4700 spectrometer.

2.3. Synthesis of metallogels based on Cd(II)–L-(+) tartaric acid (Cd–TA) and Hg(II)–L-(+) tartaric acid (Hg–TA)

The stable white Cd–TA metallogel was prepared by rapidly mixing 500 μL of a cadmium acetate DMF solution (1 mmol, 0.266 gm) with 500 μL of L(+)-tartaric acid DMF solution (2 mmol, 0.300 gm), followed by continuous ultrasonication in a water bath for ten minutes (Fig. 1). Employing the same synthetic procedure, the white stable Hg–TA metallogel was prepared by mixing 500 μL of a mercury acetate DMF solution (1 mmol, 0.318 gm) with 500 μL of L(+)-tartaric acid DMF solution (2 mmol, 0.300 gm) and subjecting it to ultrasonication for ten minutes (Fig. 1). This process induces the formation of a supramolecular network *via* non-covalent interactions between the metal ions (cadmium or mercury) and L(+)-tartaric acid in DMF solvent, resulting in the development of a stable three-dimensional structure. Ultrasonication accelerates the gelation process by enhancing the mixing and assembly of these components (Fig. 1).

2.4. Determination of the minimum critical gelation concentration (MGC) for Cd–TA and Hg–TA metallogels

We determined the minimal critical gelation concentration (MGC) of Cd–TA and Hg–TA metallogels. To ascertain the MGC of Cd–TA, we varied the concentrations of $Cd(CH_3COO)_2 \cdot 2H_2O$ and L(+)-tartaric acid within a narrow range (10–566 mg mL^{-1}), maintaining a constant molar ratio of 1 : 2 to form the Cd–TA metallogel. A stable, white-colored metallogel, Cd-CA, was obtained at a concentration of 566 mg mL^{-1} of Cd(II)-acetate salt and L(+)-tartaric acid in DMF solvent. For the evaluation of the MGC of Hg–TA metallogel, we varied the concentrations of $Hg(CH_3COO)_2$ salt and L(+)-tartaric acid (10–618 mg mL^{-1}). A stable Hg–TA metallogel was formed at a concentration of 618 mg mL^{-1} of Cd(II)-acetate salt and L(+)-tartaric acid in DMF solvent.

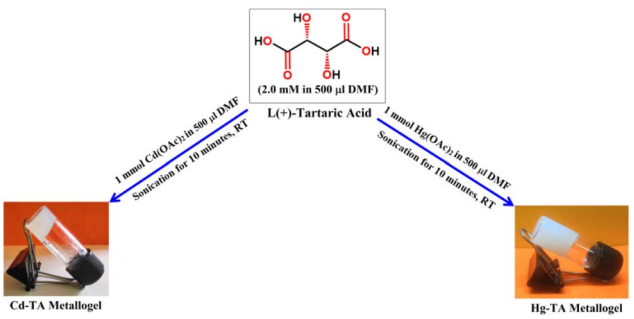

Fig. 1 Schematic representation of the synthetic route of Cd(II)-metallogel (Cd–TA) and Hg(II)-metallogel (Hg–TA).

2.5. Antimicrobial activity of metallogels

To test bacterial susceptibility to metallogels Cd–TA and Hg–TA, both were suspended in MilliQ water at a concentration of 100 mg mL^{-1}. The antibacterial activity was tested against *Escherichia coli* (*E. coli*), *Pseudomonas aeruginosa* (*P. aeruginosa*), *Bacillus subtilis* (*B. subtilis*) and *Staphylococcus epidermidis* (*S. epidermidis*). As positive control, a conventional antibiotic (streptomycin) was used. Using a sterile cotton swab, 100 μL of each bacterial inoculum (log phase culture) was evenly and independently placed over the solid surface of TGE (tryptone, glucose, yeast extract, all at 1%; pH 6.5) agar plates. 10 μL of each metallogel suspension was spotted across the surface of agar plates. The plates were incubated at 37 °C for 24 hours. The experiment was carried out in triplicates.

3. Results and discussion

3.1. Rheological analysis

To assess the mechanical stability of Cd–TA and Hg–TA metallogels, we conducted rheological analyses varying angular frequency and strain. When the storage modulus (G') surpasses the loss modulus (G''), it indicates a viscoelastic material. Both

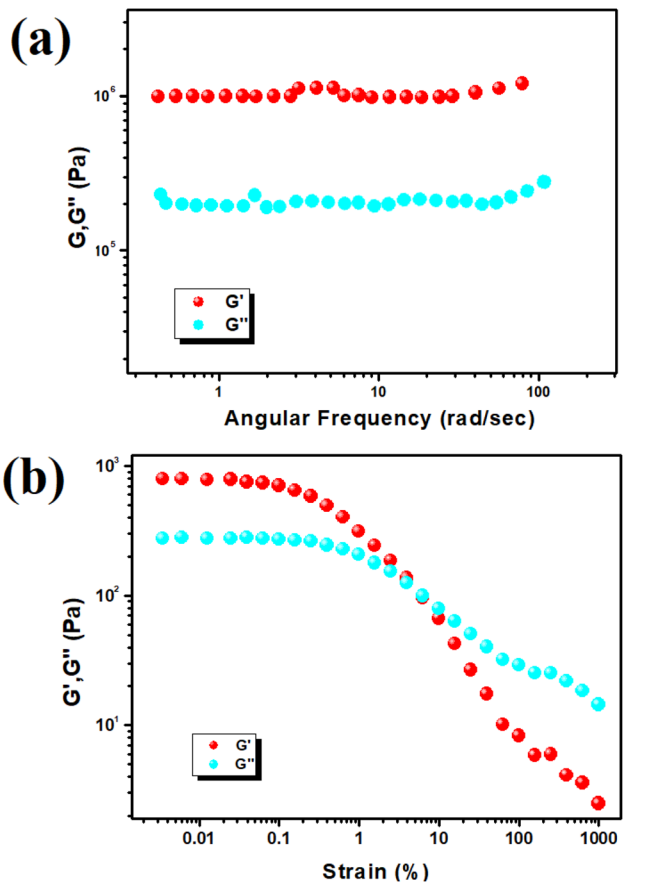

Fig. 2 (a) The graph illustrates the variation of storage modulus (G') and loss modulus (G'') of Cd(II) metallogel with angular frequency; (b) strain-sweep measurements of Cd(II) metallogel were conducted at a consistent frequency of 6.283 rad s^{-1}.

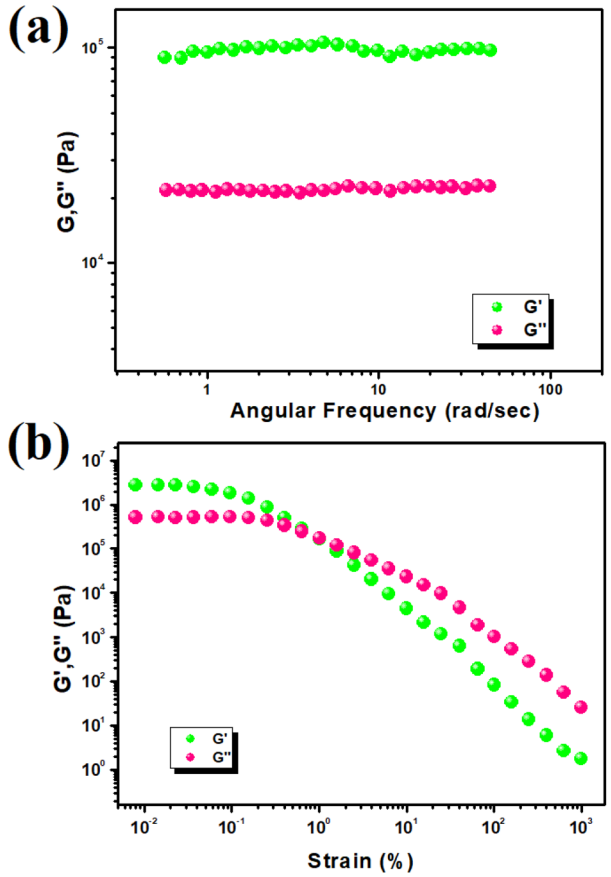

Fig. 3 (a) The figure depicts the relationship between the storage modulus (G') and loss modulus (G'') of Hg(II) metallogel as a function of angular frequency; (b) strain-sweep measurements of Hg(II) metallogel were carried out at a steady frequency of 6.27997 rad s^{-1}.

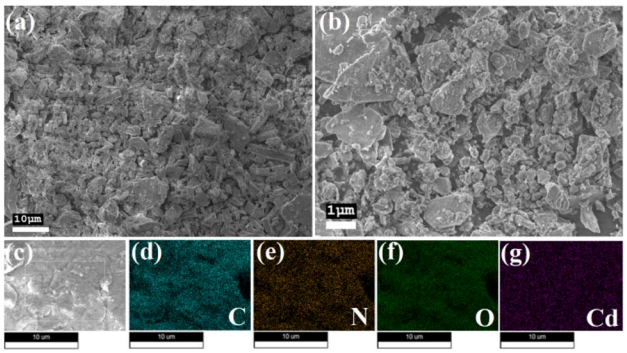

Fig. 4 (a and b) FESEM microstructural characteristics of Cd–TA metallogel; (c–g) elemental mapping of Cd–TA metallogel reveals the presence of C, N, O, and Cd elements.

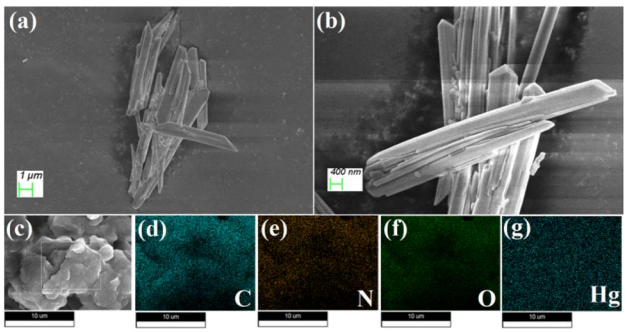

Fig. 5 (a and b) FESEM microstructural analysis of Hg–TA metallogel; (c–g) elemental mapping of Hg–TA metallogel confirms the presence of C, N, O, and Hg elements.

Cd–TA and Hg–TA metallogels exhibit semi-solid-like behavior with $G' > G''$, confirming their gel nature. Cd–TA metallogel demonstrates high tolerance, evident in its average storage modulus ($G' > 10^6$ Pa) far exceeding its loss modulus (G'') (Fig. 2a). The strain-sweep measurement of Cd–TA metallogel at a fixed frequency of 6.283 rad s^{-1} is depicted in Fig. 2b. In experiments with Hg–TA metallogel at a consistent concentration of $Hg(CH_3COO)_2$ salt and L(+)-tartaric acid (MGC = 618 mg mL^{-1}), the storage modulus (G') significantly exceeds the loss modulus (G'') (*i.e.*, $G' > G''$) (Fig. 3a). This reaffirms the gel-like structure and solid-like behavior of Hg–TA metallogel, as illustrated by the rheological data. Notably, the average storage modulus (G') considerably outweighs the loss modulus (G'') (Fig. 3a). Fig. 3b showcases a strain-sweep experiment conducted on Hg–TA metallogel at a constant frequency of 6.27997 rad s^{-1}. The results reveal that the critical strain, marking the onset of gel breakdown for Hg–TA metallogel, occurs at a strain of 0.45%, where G' merges with G'' (Fig. 3b).

3.2. Study of morphology

The morphological characteristics of Cd–TA and Hg–TA metallogels were investigated using field-emission scanning electron microscopy (FESEM) images. In the FESEM images of Cd–TA metallogel, a distinct network resembling agglomerated rock-like structures was prominent (Fig. 4a–d). This architecture resulted from the interaction between $Cd(CH_3COO)_2 \cdot 2H_2O$ and L(+)-tartaric acid in a DMF medium, as observed in the FESEM patterns. Supramolecular interactions between $Cd(CH_3COO)_2 \cdot 2H_2O$ and L(+)-tartaric acid in DMF facilitated the formation of these microstructural networks. Elemental mapping through energy-dispersive X-ray spectroscopy (EDX) confirmed the presence of C, Cd, N, and O elements in Cd–TA metallogel (Fig. 4e–i). Similarly, FESEM analysis of Hg–TA metallogel revealed agglomerated nano-rod-like structures (Fig. 5a–d), with EDX elemental mapping confirming the presence of C, N, O, and Hg elements as the main constituents of Hg–TA metallogel (Fig. 5e–i).

3.3. FT-IR analysis of Cd–TA and Hg–TA metallogels

To characterize the synthesized Cd–TA and Hg–TA metallogels, Fourier Transform Infrared (FT-IR) spectroscopy was performed due to its sensitivity to different functional groups. The FT-IR spectra of the xerogel forms of Cd–TA and Hg–TA metallogels reveal the supramolecular interactions between tartaric acid and the Cd(II) and Hg(II) sources, which are responsible for the formation of the metallogels (Fig. S1 and S2†). Functional groups present in the material exhibit characteristic vibrations,

serving as fingerprints for identification. These vibration bands undergo shifts to shorter or longer wavelengths depending on changes in the material's microenvironment.

In Cd–TA metallogel, significant spectral absorption bands include the O–H stretching of hydroxyl groups are observed as peaks at 3360 cm^{-1} and 3130 cm^{-1} (Fig. S1†). The vibrational mode at 2940 cm^{-1} and 2800 cm^{-1} corresponds to symmetric C–H bonds. The carboxyl C=O stretching in the carboxyl group is associated with peaks at 1720 cm^{-1}. Vibrational modes linked to peaks at 1630 cm^{-1}, 1390 cm^{-1}, and 1270 cm^{-1} represent N–O stretching, C–N stretching, and C–O stretching, respectively. Additionally, peaks at 985 cm^{-1}, 1060 cm^{-1} indicates the presence of the Cd–O bond, further confirming the connection between L(+)-tartaric acid and DMF-soluble cadmium acetate.[65]

Similarly, in Hg–TA metallogel, significant spectral absorption bands include the O–H stretching of hydroxyl groups, visible as a broad peak at 3460 cm^{-1} (Fig. S2†). The vibrational mode at 2980 cm^{-1} corresponds to symmetric C–H bonds. The carboxyl C=O stretching in the carboxyl group is associated with peaks at 1730 cm^{-1}. Vibrational modes associated with peaks at 1610 cm^{-1}, 1400 cm^{-1}, and 1260 cm^{-1} represent N–O stretching, C–N stretching, and C–O stretching, respectively. Furthermore, a peak at 618 cm^{-1} confirms the presence of the Hg–O bond, strengthening the connection between L(+)-tartaric acid and DMF-soluble mercury acetate. Please see the ESI† for UV-vis absorption spectra of Cd–TA and Hg–TA metallogel as Fig. S3 and S4.†

3.4. PXRD analysis of Cd–TA and Hg–TA metallogels

Powder X-ray diffraction was used to examine the nature of the Cd–TA metallogel (Fig. 6a). At particular 2θ values, the diffraction pattern showed twelve distinct sharp peaks: 11.16° 13.94°, 16.59°, 21.87°, 32°, 37.88°, 40.23°, 44.19°, 48.59°, 51.37°, 56.81°, 57.54°, 66.20° respectively. The sharp peaks show that the synthesized chemical has a high degree of crystallinity. Cd acetate monohydrate and L(+)-tartaric acid were found to be present based on the room temperature XRD patterns. In particular, the values of 2θ were found to correlate to several substances: 11.16°, 13.94°, 16.59° correspond to both $Cd(OAc)_2 \cdot H_2O$ and $Cd(OAc)_2$; tartaric acid was associated with 21.87°, 32°, 37.88°, 40.23°; and other remaining peaks correspond to DMF solvent.

Powder X-ray diffraction was used to analyze the Hg–TA metallogel's composition (Fig. 6b). Twenty three distinct peaks were visible in the diffraction pattern at particular 2θ values: 11.59°, 14.97°, 16.89°, 17.76°, 21.59°, 23.05°, 25.25°, 27.30°, 29.22°, 33.18°, 34.50°, 36.40°, 38.16°, 42.43°, 46.09°, 50.49°, 53.72°, 56.96°, 59.75°, 61.22°, 63.57°, 71.20°, 73.25° respectively. Among these peaks, sixteen peaks are sharp and other remaining peaks were narrow. These sharp peaks show that the produced chemical has a high amount of crystallinity. Tartaric acid and Hg acetate monohydrate were found by examining the room temperature XRD patterns. In particular, the values of 2θ correlated with $(Hg(OAc)_2 \cdot H_2O)$ at 11.59°, 14.97°, 16.89°, 17.76°; $(Hg(OAc)_2)$ corresponds to 21.59°, 23.05°, 25.25°, 27.30°, 29.22°; L(+)-tartaric acid corresponds to 33.18°, 34.50°, 36.40°, 38.16°, 42.43°, 46.09°; and other remaining peaks correspond to DMF solvent.

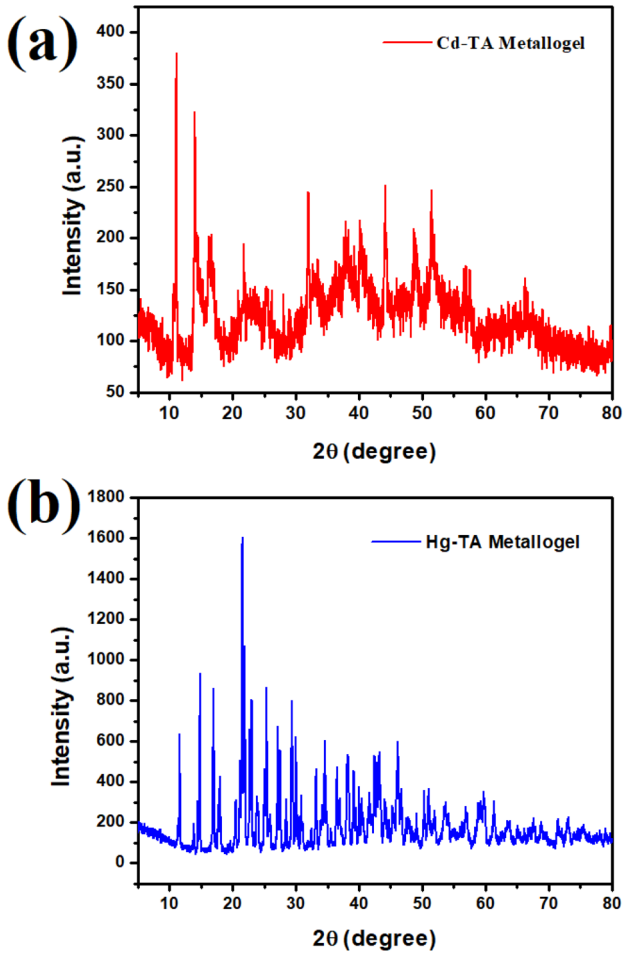

Fig. 6 (a and b) PXRD spectra of Cd–TA and Hg–TA metallogel in their xerogel form.

3.5. Inhibiting activity for pathogens

Introducing metal components into gel matrices is an efficient technique for developing soft materials with an enhanced antimicrobial activity. Recent developments in natural and synthetic hydrogels have either inherent antibacterial characteristics or they may also act as an antibiotic carrier. Given the misuse of antibiotics and other antimicrobial drugs, metallogel may be a feasible alternative to current antibiotic therapy.

Fig. 7 shows the antimicrobial activity of Cd–TA and Hg–TA against four pathogenic strains (a) *E. coli*, (b) *P. aeruginosa*, (c) *B. subtilis* and (d) *S. epidermidis*. Clear zones indicate effective inhibition of bacterial growth. Over time, metallogels diffused into agar medium and inhibited the growth of the bacteria. Table 1 shows the effectiveness of streptomycin (positive control antibiotic), Cd–TA, and Hg–TA against four different bacterial strains. The size of the clear zone around each treatment (in millimeters) indicates how well it inhibits bacterial growth. The antibacterial potency of Hg–TA was determined to be higher than that of Cd–TA. The formation of inhibitory zones following

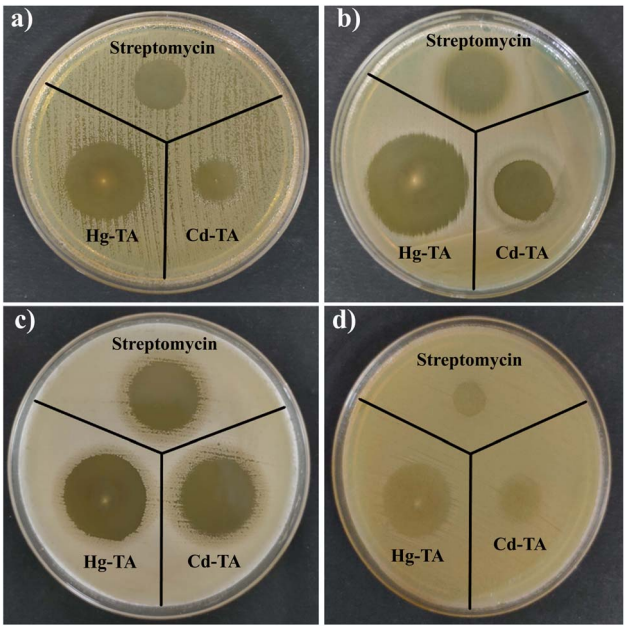

Fig. 7 Antimicrobial activity of Cd–TA and Hg–TA against four pathogenic strains (a) *E. coli*, (b) *P. aeruginosa*, (c) *B. subtilis* and (d) *S. epidermidis*.

Table 1 Antimicrobial activity of metallogels[a]

Bacterial strain (s)	Zone of inhibition against streptomycin (mm in diameter)
E. coli	16.83 ± 0.76
P. aeruginosa	20.16 ± 0.28
B. subtilis	20.83 ± 0.76
S. epidermidis	11.5 ± 0.5

Bacterial strains (s)	Volume of metallogel (μL)	Concentration of metallogel (mg mL^{-1})	Zone of inhibition (mm in diameter)	
			Cd–TA	Hg–TA
E. coli	10	100	16.5 ± 0.5	24.83 ± 0.28
P. aeruginosa	10	100	18.83 ± 0.76	32.5 ± 0.5
B. subtilis	10	100	23.5 ± 0.5	25.83 ± 0.76
S. epidermidis	10	100	12.33 ± 0.76	21.16 ± 0.76

[a] ± standard deviation.

contact with metallogels suggests that they have the potential to be utilized as broad-spectrum antimicrobial agents. In antimicrobial susceptibility test, the zone of inhibition around the positive control antibiotic serves as a benchmark to evaluate the effectiveness of synthesized derivatives. On an agar plate, a substance with antimicrobial properties creates a clear zone around itself. This zone indicates the area where the substance stops bacterial growth. Synthesized derivatives are considered promising if their zones of inhibition are comparable with the control antibiotic. A smaller inhibition zone compared to streptomycin does not negate the antimicrobial properties of synthesized derivatives. They still possess antimicrobial activity, just less potent than streptomycin at this specific concentration. But this may be very useful for controlled drug treatment, where a relatively low inhibitory drugs are required.

4. Conclusions

In summary, this study successfully synthesized innovative metallogels by directly mixing cadmium acetate dihydrate and mercury acetate solutions with L(+)-tartaric acid, followed by ultrasonication at room temperature. FESEM analysis revealed distinct morphological patterns in Cd(II) and Hg(II)-based metallogels. Rheological tests confirmed their mechanical stability, while FT-IR spectroscopy provided insights into potential intermolecular interactions within the gel structures. Both Cd(II) and Hg(II)-metallogels showed significant potential in inhibiting harmful bacteria, as demonstrated by antibacterial assays, particularly in biomedicine and pharmaceuticals. These materials offer innovative solutions for combating bacterial infections and addressing critical healthcare challenges. The developed synthesis protocol holds promise for further exploration and application. Overall, this study offers a transformative pathway for advancements in science and technology, with far-reaching societal benefits.

Data availability

The authors declare that the data supporting the findings of this study are available within the paper and its ESI.† Should any raw data files be needed in another format they are available from the corresponding author upon reasonable request.

Conflicts of interest

The authors declare no competing financial interests.

Acknowledgements

S. D. is grateful to the UGC, New Delhi, for awarding him Dr DS Kothari Postdoctoral Fellowship (award letter number: F.4-2/2006 (BSR)/CH/19-20/0224). S. P. acknowledges University Grants Commission (UGC), Government of India for Senior Research Fellowship (award letter number: 16-6(DEC.2018)/2019(NET/CSIR)). S. B. thankfully acknowledges DST Inspire Faculty Research Grant (Faculty Registration No. IFA18-CH304; DST/INSPIRE/04/2018/000329).

Notes and references

1 D. Tripathy, A. S. Gadtya and S. Moharana, *Polym.-Plast. Technol. Mater.*, 2023, **62**, 306–326.
2 S. Datta and S. Bhattacharya, *Chem. Soc. Rev.*, 2015, **44**, 5596–5637.
3 A. Pape, M. Bastings, R. Kieltyka, H. Wyss, I. Voets, E. Meijer and P. Dankers, *Int. J. Mol. Sci.*, 2014, **15**, 1096–1111.

4 S. Dhibar, H. Dahiya, K. Karmakar, S. Kundu, S. Bhattacharjee, G. C. Nayak, P. Karmakar, G. D. Sharma and B. Saha, *J. Mol. Liq.*, 2023, **370**, 121020.
5 K. Karmakar, A. Dey, S. Dhibar, R. Sahu, S. Bhattacharjee, P. Karmakar, P. Chatterjee, A. Mondal and B. Saha, *RSC Adv.*, 2023, **13**, 2561–2569.
6 S. Ganta and D. K. Chand, *Dalton Trans.*, 2015, **44**, 15181–15188.
7 G. Yu, X. Yan, C. Han and F. Huang, *Chem. Soc. Rev.*, 2013, **42**, 6697.
8 S. Dhibar, S. K. Ojha, A. Mohan, S. P. C. Prabhakaran, S. Bhattacharjee, K. Karmakar, P. Karmakar, P. Predeep, A. K. Ojha and B. Saha, *New J. Chem.*, 2022, **46**, 17189–17200.
9 M. Shirakawa, N. Fujita and S. Shinkai, *J. Am. Chem. Soc.*, 2003, **125**, 9902–9903.
10 T.-A. Asoh and A. Kikuchi, *Chem. Commun.*, 2012, **48**, 10019.
11 X. Yang, H. Zhang, J. Zhao, Y. Liu, Z. Zhang, Y. Liu and X. Yan, *Chem. Eng. J.*, 2022, **450**, 138135.
12 A. Rajak and A. Das, *ACS Polym. Au*, 2022, **2**, 223–231.
13 Y. Xu, Q. Wu, Y. Sun, H. Bai and G. Shi, *ACS Nano*, 2010, **4**, 7358–7362.
14 S. Dhibar, S. K. Ojha, A. Mohan, S. P. C. Prabhakaran, S. Bhattacharjee, K. Karmakar, P. Karmakar, P. Predeep, A. K. Ojha and B. Saha, *New J. Chem.*, 2022, **46**, 17189–17200.
15 J. W. Steed, *Chem. Soc. Rev.*, 2010, **39**, 3686.
16 K. Hanabusa, K. Hiratsuka, M. Kimura and H. Shirai, *Chem. Mater.*, 1999, **11**, 649–655.
17 A. Prathap and K. M. Sureshan, *Langmuir*, 2019, **35**, 6005–6014.
18 N. Shi, G. Yin, H. Li, M. Han and Z. Xu, *New J. Chem.*, 2008, **32**, 2011.
19 S. J. Wezenberg, C. M. Croisetu, M. C. A. Stuart and B. L. Feringa, *Chem. Sci.*, 2016, **7**, 4341–4346.
20 M.-O. M. Piepenbrock, G. O. Lloyd, N. Clarke and J. W. Steed, *Chem. Rev.*, 2010, **110**, 1960–2004.
21 S. Dhibar, A. Dey, A. Dey, S. Majumdar, D. Ghosh, P. P. Ray and B. Dey, *ACS Appl. Electron. Mater.*, 2019, **1**, 1899–1908.
22 (*a*) S. Dhibar, A. Dey, S. Majumdar, D. Ghosh, A. Mandal, P. P. Ray and B. Dey, *Dalton Trans.*, 2018, **47**, 17412–17420; (*b*) S. Dhibar, A. Dey, D. Ghosh, S. Majumdar, A. Dey, P. Mukherjee, A. Mandal, P. P. Ray and B. Dey, *ChemistrySelect*, 2019, **4**, 1535–1541; (*c*) S. Dhibar, A. Dey, S. Majumdar, A. Dey, P. P. Ray and B. Dey, *Ind. Eng. Chem. Res.*, 2020, **59**, 5466–5473; (*d*) S. Dhibar, A. Dey, S. Majumdar, P. P. Ray and B. Dey, *Int. J. Energy Res.*, 2021, **45**, 5486–5499; (*e*) S. Dhibar, S. K. Ojha, A. Mohan, S. P. C. Prabhakaran, S. Bhattacharjee, K. Karmakar, P. Karmakar, P. Predeep, A. K. Ojha and B. Saha, *New J. Chem.*, 2022, **46**, 17189–17200; (*f*) S. Dhibar, H. Dahiya, K. Karmakar, S. Kundu, S. Bhattacharjee, G. C. Nayak, P. Karmakar, G. D. Sharma and B. Saha, *J. Mol. Liq.*, 2023, **370**, 121020; (*g*) S. Dhibar, A. Dey, A. Dalal, S. Bhattacharjee, R. Sahu, R. Sahoo, A. Mondal, S. M. Rahaman, S. Kundu and B. Saha, *J. Mol. Liq.*, 2023, **370**, 121021; (*h*) S. Dhibar, S. Babu, A. Mohan, G. K. Chandra, S. Bhattacharjee, K. Karmakar, P. Karmakar, S. M. Rahaman, P. Predeep and B. Saha, *J. Mol. Liq.*, 2023, **375**, 121348; (*i*) K. Karmakar, A. Dey, S. Dhibar, R. Sahu, S. Bhattacharjee, P. Karmakar, P. Chatterjee, A. Mondal and B. Saha, *RSC Adv.*, 2023, **13**, 2561–2569; (*j*) S. Dhibar, B. Pal, K. Karmakar, S. Kundu, S. Bhattacharjee, R. Sahoo, S. M. Rahaman, D. Dey, P. P. Ray and B. Saha, *ChemistrySelect*, 2023, **8**, e202204214.
23 S. Ganta and D. K. Chand, *Dalton Trans.*, 2015, **44**, 15181–15188.
24 X.-Q. Wang, W. Wang, G.-Q. Yin, Y.-X. Wang, C.-W. Zhang, J.-M. Shi, Y. Yu and H.-B. Yang, *Chem. Commun.*, 2015, **51**, 16813–16816.
25 C. Po, Z. Ke, A. Y. Tam, H. Chow and V. W. Yam, *Chem.–Eur. J.*, 2013, **19**, 15735–15744.
26 B. Jiang, L.-J. Chen, G.-Q. Yin, Y.-X. Wang, W. Zheng, L. Xu and H.-B. Yang, *Chem. Commun.*, 2017, **53**, 172–175.
27 C. A. Offiler, C. D. Jones and J. W. Steed, *Chem. Commun.*, 2017, **53**, 2024–2027.
28 Z. Yao, Z. Wang, Y. Yu, C. Zeng and K. Cao, *Polymer*, 2017, **119**, 98–106.
29 K. Mitsumoto, J. M. Cameron, R. Wei, H. Nishikawa, T. Shiga, M. Nihei, G. N. Newton and H. Oshio, *Chem.–Eur. J.*, 2017, **23**, 1502–1506.
30 Y. Lan, M. G. Corradini, R. G. Weiss, S. R. Raghavan and M. A. Rogers, *Chem. Soc. Rev.*, 2015, **44**, 6035–6058.
31 G. Deng, F. Li, H. Yu, F. Liu, C. Liu, W. Sun, H. Jiang and Y. Chen, *ACS Macro Lett.*, 2012, **1**, 275–279.
32 S. Das, M. Banik, G. Chen, S. Sinha and R. Mukherjee, *Soft Matter*, 2015, **11**, 8550–8583.
33 M. r. Saboktakin and R. M. Tabatabaei, *Int. J. Biol. Macromol.*, 2015, **75**, 426–436.
34 Y. Zhao, S. Song, X. Ren, J. Zhang, Q. Lin and Y. Zhao, *Chem. Rev.*, 2022, **122**, 5604–5640.
35 Y. Xu, Q. Wu, Y. Sun, H. Bai and G. Shi, *ACS Nano*, 2010, **4**, 7358–7362.
36 A. R. Hirst, B. Escuder, J. F. Miravet and D. K. Smith, *Angew. Chem., Int. Ed.*, 2008, **47**, 8002–8018.
37 S. Sarkar, S. Dutta, S. Chakrabarti, P. Bairi and T. Pal, *ACS Appl. Mater. Interfaces*, 2014, **6**, 6308–6316.
38 P. Terech, M. Yan, M. Maréchal, G. Royal, J. Galvez and S. K. P. Velu, *Phys. Chem. Chem. Phys.*, 2013, **15**, 7338.
39 C. Mahendar, Y. Kumar, M. K. Dixit and M. Dubey, *Soft Matter*, 2020, **16**, 3436–3442.
40 S. Dhibar, A. Dey, A. Dey, S. Majumdar, D. Ghosh, P. P. Ray and B. Dey, *ACS Appl. Electron. Mater.*, 2019, **1**, 1899–1908.
41 S. Dhibar, A. Dey, S. Majumdar, D. Ghosh, A. Mandal, P. P. Ray and B. Dey, *Dalton Trans.*, 2018, **47**, 17412–17420.
42 N. Maldonado and P. Amo-Ochoa, *Nanomaterials*, 2021, **11**, 1865.
43 S. Dhibar, S. K. Ojha, A. Mohan, S. P. C. Prabhakaran, S. Bhattacharjee, K. Karmakar, P. Karmakar, P. Predeep, A. K. Ojha and B. Saha, *New J. Chem.*, 2022, **46**, 17189–17200.
44 (*a*) B. Pal, S. Dhibar, R. Mukherjee, S. Bhattacharjee, P. P. Ray and B. Saha, *Mater. Adv.*, 2023, **4**, 3628–3635; (*b*) S. Dhibar, S. K. Ojha, K. Karmakar, P. Karmakar, S. Bhattacharjee, P. Chatterjee, A. K. Ojha and B. Saha, *Chem. Afr.*, 2023, **6**, 3217–3228.

45 S. Dhibar, S. Babu, K. Karmakar, A. Mohan, S. Bhattacharjee, S. M. Rahaman, G. C. Nayak, R. Saha, P. Predeep and B. Saha, *Chem. Phys. Lett.*, 2023, **829**, 140777.
46 (*a*) K. Karmakar, A. Dey, S. Dhibar, R. Sahu, S. Bhattacharjee, P. Karmakar, P. Chatterjee, A. Mondal and B. Saha, *RSC Adv.*, 2023, **13**, 2561–2569; (*b*) A. Roy, S. Dhibar, K. Karmakar, S. Some, S. A. Hafiz, S. Bhattacharjee, B. Saha and S. J. Ray, *Mater. Adv.*, 2024, **5**, 3459–3471.
47 J. Chen, T. Wang and M. Liu, *Inorg. Chem. Front.*, 2016, **3**, 1559–1565.
48 S. Dhibar, S. Pal, K. Karmakar, S. A. Hafiz, S. Bhattacharjee, A. Roy, S. K. M. Rahaman, S. J. Ray, S. Dam and B. Saha, *RSC Adv.*, 2023, **13**, 32842–32849.
49 S. Dhibar, S. Pal, K. Karmakar, S. A. Hafiz, S. Bhattacharjee, A. Roy, S. K. M. Rahaman, S. J. Ray, S. Dam and B. Saha, *RSC Adv.*, 2023, **13**, 32842–32849.
50 E. M. M. Ibrahim, L. H. Abdel-Rahman, A. M. Abu-Dief, A. Elshafaie, S. K. Hamdan and A. M. Ahmed, *Mater. Res. Bull.*, 2018, **107**, 492–497.
51 W.-L. Guan, K. M. Adam, M. Qiu, Y.-M. Zhang, H. Yao, T.-B. Wei and Q. Lin, *Supramol. Chem.*, 2020, **32**, 578–596.
52 E. M. M. Ibrahim, L. H. Abdel-Rahman, A. M. Abu-Dief, A. Elshafaie, S. K. Hamdan and A. M. Ahmed, *Mater. Res. Bull.*, 2018, **107**, 492–497.
53 N. Malviya, C. Sonkar, R. Ganguly, D. Bhattacherjee, K. P. Bhabak and S. Mukhopadhyay, *ACS Appl. Mater. Interfaces*, 2019, **11**, 47606–47618.
54 B. C. Roy, A. Kundu, P. Biswas, S. Roy and T. S. Mahapatra, *ChemistrySelect*, 2024, **9**, e202304755.
55 D. Bairagi, P. Ghosh, P. Roy and A. Banerjee, *ACS Appl. Nano Mater.*, 2023, **6**, 2299–2309.
56 G. Lepcha, S. Majumdar, B. Pal, K. T. Ahmed, I. Pal, B. Satpati, S. R. Biswas, P. P. Ray and B. Dey, *Langmuir*, 2023, **39**, 7469–7483.
57 G. Lepcha, B. Pal, S. Majumdar, K. T. Ahmed, I. Pal, S. R. Biswas, P. P. Ray and B. Dey, *Mater. Adv.*, 2023, **4**, 2595–2603.
58 H. T. P. Anh, C.-M. Huang and C.-J. Huang, *Sci. Rep.*, 2019, **9**, 11562.
59 S. Dhibar, A. Dey, A. Dalal, S. Bhattacharjee, R. Sahu, R. Sahoo, A. Mondal, S. M. Rahaman, S. Kundu and B. Saha, *J. Mol. Liq.*, 2023, **370**, 121021.
60 L. Coppola, D. Coffetti and E. Crotti, *Constr. Build. Mater.*, 2018, **171**, 243–249.
61 I. Begum, S. Shamim, F. Ameen, Z. Hussain, S. A. Bhat, T. Qadri and M. Hussain, *Processes*, 2022, **10**, 716.
62 A. A. A. Aziz, F. M. Elantabli, H. Moustafa and S. M. El-Medani, *J. Mol. Struct.*, 2017, **1141**, 563–576.
63 A. Al-Ghafari, E. Elmorsy, E. Fikry, M. Alrowaili and W. G. Carter, *PLoS One*, 2019, **14**, e0225341.
64 I.-L. Steffensen, O. J. Mesna, E. Andruchow, E. Namork, K. Hylland and R. A. Andersen, *Gen. Pharmacol.*, 1994, **25**, 1621–1633.
65 S. Kumar, B. Ahmed, A. K. Ojha, J. Das and A. Kumar, *Mater. Res. Bull.*, 2017, **90**, 224–231.